A numerical study of AC electroosmosis

Tom E. de Vries

June 2021

Supervisor: René van Roij   Institute for Theoretical Physics

Abstract

AC electroosmosis is the process in which fluid flows are induced by oscillating electric fields. When the ions in the fluid have different sizes or valencies, the application of an oscillating field can give rise to non-zero average fields called Asymmetric Rectified Electric Fields (AREFs). We study the properties of AREFs in a one dimensional system of two planar electrodes. We use Numerical methods to solve the Poisson-Nernst-Planck equations and measure the average electric potential as a function of system size, driving frequency, driving amplitude, and the valencies and diffusivities of the ions. If diffusivities are unequal but valencies are not, we find that the average potential scales with the square of the driving frequency in the low frequency regime. We also find that the average potential changes sign at a particular frequency related to the system size. If valencies are unequal but diffusivities are not, the sign change persists, but the average potential stays constant at low frequencies. This constant value increases with the driving amplitude and valency difference.

Contents

1 Introduction

In this work we will investigate the behaviour of electrolytes in oscillating electric fields. This behaviour is of particular interest to the field of ac electroosmosis (ACEO) [1], which describes the way fluids move under oscillating potentials. ACEO in turn has applications in lab-on-a-chip (LOC) systems, which are small chips that perform one or more laboratory functions [2]. While they are still relatively difficult to produce, their small size makes for fast response times and easy control of temperature and other variables. Other advantages include the low cost in raw material for manufacture and the low requirements for reagents, which also leads to low waste output [3]. One problem faced by LOCs is how to effectively control the flow of fluids. Here, ACEO holds a possible solution. By using oscillating electric fields, it is possible to pump fluid through the chip without any moving parts [2][4][5].

Of particular interest is the behaviour electrolytes consisting of ions with significantly different shapes or sizes, leading to different diffusion constants. Such systems have been shown to give rise to so-called Asymmetric Rectified Electric Fields (AREFs) [6]. When these AREFs are present, the average of the total potential over a period of the oscillation can become non-zero. This can give rise to unexpected flow patterns [7]. We want to find out how the value of this non-zero potential changes as a function of several system parameters such as the system size, oscillation frequency, and the relative diffusion coefficients and charges of the positive and negative ions. We wrote a computer program to solve the relevant equations without the need to linearise them. While some research into the properties of AREFs exists [8][9], we want to place further emphasis on frequency dependence and the effects of having different ionic valencies. We will see that when the ionic diffusion constants are different from each other, the average potential increases with the square of the driving frequency before reaching a maximum at a characteristic frequency. It then decays to zero at a second characteristic frequency related to the system size. We will also find that if the ionic valencies are different from each other, the average potential stays constant until the first characteristic frequency, after which it also decays to zero at the second characteristic frequency.

2 Theory

The system of interest is that of an electrolyte between two planar electrodes separated by a distance L. Note that we chose to place the electrodes at 0 and L. In some other works, the electrodes are placed at $-l$ and l, so the distance between them would be $2l$ [8]. Because the electrodes are assumed to be macroscopically large, we can assume translational invariance in the plane parallel to the electrodes, and we can treat this as a one-dimensional problem. Before discussing our system, we need to go over a few important concepts.
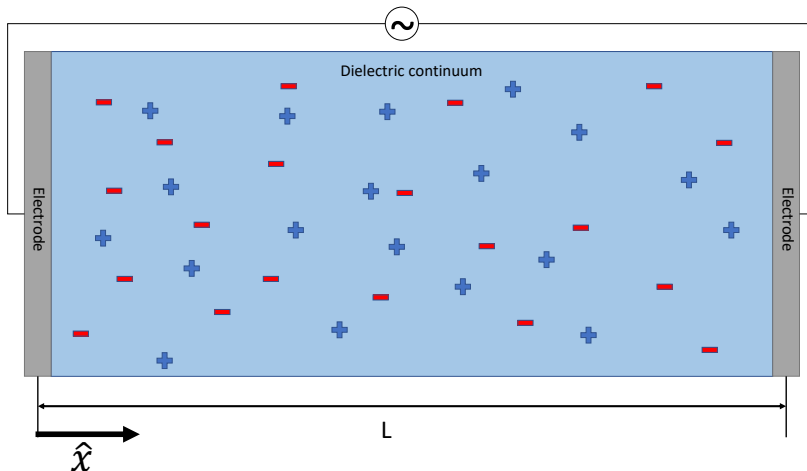
Figure 1: A schematic representation of the system. Two electrodes are separated by a distance L, the space between them contains an electrolyte that we treat as a continuum.

2.1 Electric Double Layers

Before we move on to describing our system, we first need to go over the concept of the electric double layer (EDL). To demonstrate what an EDL is and why it forms we focus on a slightly different system shown in figure 2. This system has only one macroscopically large electrode. We assume the electrolyte extends into the far distance so we can assume the potential and densities take constant bulk values far from the electrode.

For now, we will assume a 1:1 electrolyte in which the positive and negative ions are identical aside from the sign of their charge. We do not describe the individual ions, instead we use number densities in our calculations. We will apply a static potential to the electrode. To describe this system, we will use the
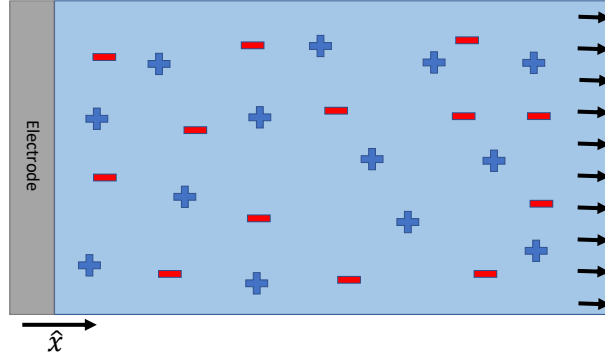
Figure 2: A schematic representation of the system used to demonstrate EDLs. There is an electrode at one end, and an open boundary at the other. The open boundary is represented by arrows.

Poisson-Boltzmann equations [10]. The first of these equations is the Poisson equation:

$$\phi''(x) = -\frac{e}{\epsilon}(n_+(x) - n_-(x)), \tag{1}$$

where ϕ is the electric potential, primes denote derivatives with respect to x, $n_\pm$ is the number density of the monovalent cations/anions, e is the elementary charge, and ϵ is the dielectric permittivity of the solvent. The number densities in the static case are given by the mean-field Boltzmann distributions:

$$n_\pm(x) = n_s \exp\left(\mp\frac{e\phi(x)}{k_B T}\right). \tag{2}$$

Here, n_s is the bulk density, T is the temperature, and k_B is Boltzmann's constant. Eqs.(1) and (2) form a second order differential equation. Such an equation requires two boundary conditions to solve. For the first boundary condition, we choose the zero point in our potential to be the value in the bulk of the electrolyte:

$$\phi(x \to \infty) = 0. \tag{3}$$

The second boundary condition comes from the static potential we apply to the electrode, which we place at $x = 0$.

$$\phi(x = 0) = \Phi_0. \tag{4}$$

We can combine equations (1) and (2) and define $\tilde{\phi} = \frac{\phi e}{k_B T}$ to write:

$$\frac{d^2\tilde{\phi}(x)}{dx^2} = \frac{e^2 n_s}{\epsilon k_B T} \sinh(\tilde{\phi}(x)) = \kappa^2 \sinh(\tilde{\phi}(x)). \tag{5}$$

Here, $\kappa^{-1} = \sqrt{\frac{\epsilon k_B T}{e^2 n_s}}$ is the Debye length. We will discuss its significance later on. Eq.(5) can be solved analytically in its full form, but for this demonstration

it suffices to solve a linearised version where we assume $|\tilde{\phi}| \ll 1$:

$$\frac{d^2\tilde{\phi}(x)}{dx^2} \approx \kappa^2 \tilde{\phi}(x). \tag{6}$$

The solution to eq.(6) takes the form:

$$\tilde{\phi}(x) = Ae^{-\kappa x} + Be^{\kappa x}. \tag{7}$$

Applying the first boundary condition (eq.(3)) gives us $\lim_{x \to \infty} Be^{\kappa x} = 0$, which implies $B = 0$. Next, applying the second boundary condition (eq.(4)) gives us $A = \tilde{\Phi}_0$. This means the linearised solution to the Poisson-Boltzmann equations is:

$$\tilde{\phi}(x) = \tilde{\Phi}_0 e^{-\kappa x} \qquad n_\pm = n_s(1 \mp \tilde{\Phi}_0 e^{-\kappa x}). \tag{8}$$

The potential and densities described in eq.(8) are shown in figure 3.
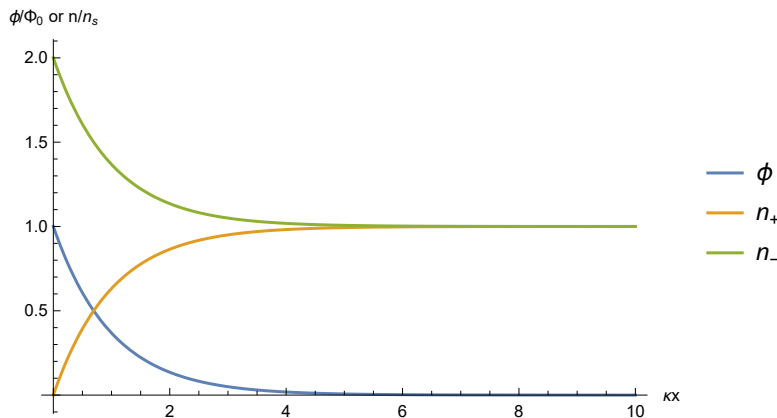
Figure 3: The static solution to the linearised Poisson-Boltzmann equations for the electric potential ϕ and number densities of the cations (n_+) and anions (n_-). Near the electrode, a layer of anions forms to balance the charge on the electrode. We set Φ_0 to $1V$ and n_s to $1m^{-3}$ for demonstrative purposes.

As we move away from the electrode, the potential decays exponentially. If $\tilde{\Phi}_0 > 1$, a layer of excess anions forms near the electrode to balance out the charge that is present on the electrode to induce the potential. This layer is called the Electric Double layer. The thickness of this layer is characterised by the Debye length. The concept of EDLs will be important to understanding the behaviours seen in later parts of this work.

2.2   Asymmetric Rectified Electric Fields

In section 1 we briefly mentioned the existence of Asymmetric Rectified Electric Fields (AREFs). In this section we will explain the concept in a bit more detail. This is meant to show intuitively how such a field can come to be. Our explanation is largely based on that by Amrei et al.[6].

To form an intuition about the macroscopic case, we look at a microscopic version of two individual charged particles in a quasi-one-dimensional system. Meaning the system is three dimensional, but the forces are set up so that all motion happens in one direction. This simpler model ignores diffusion and interactions between particles, but it should give an intuition as to why AREFs form. We place the two particles in an oscillating electric field:

$$E(t) = E_0 \sin(\omega t). \tag{9}$$

We assume that the particles experience only the Coulomb force from this electric field, as well as a linear drag force due to the viscosity of the solvent. We can balance these forces to get an equation of motion for the positions $(x_\pm(t))$ of each of the particles:

$$C_\pm \frac{dx_\pm}{dt} = z_\pm e E_0 \sin(\omega t). \tag{10}$$

Here, $x_\pm$ is the position of the ion, $z_\pm$ is the valency of the ion, e is the elementary charge, and $C_\pm$ is a drag coefficient. The drag coefficient $C_\pm$ is inversely proportional to the diffusion constant we will introduce later. In this section, we are interested in the case where $z_+ = -z_- = 1$. Assuming $x_\pm(t = 0) = 0$, eq.(10) can be solved to give:

$$x_\pm(t) = \mp \frac{eE_0}{C_\pm \omega} \cos(\omega t). \tag{11}$$

If $C_+ = C_-$ there is no interesting behaviour, as both particles effectively make the same movements. We are interested in the case where $C_+ \neq C_-$. The moving charges will induce a perturbation of the electric field.

We will now calculate the perturbation of the electric field at a point x_f far from both charges. We do this by performing a Taylor expansion on Coulombs law:

$$E_f(t) = \frac{kez_+}{(x_f - x_+(t))^2} + \frac{kez_-}{(x_f - x_-(t))^2}, \tag{12}$$

where $k = \frac{1}{4\pi\epsilon_0}$ is Coulombs constant and $E_f(t) = E(x_f, t)$. Remembering that $z_+ = -z_- = 1$, we can expand eq.(12) to second order in the limit of $\frac{x_\pm}{x_f} \to 0$ to get:

$$E_f(t) \approx \frac{ke}{x_f^2} + \frac{-ke}{x_f^2} + (-2)\frac{ke}{x_f^3}(-x_+(t) + x_-(t)) + 3\frac{ke}{x_f^4}\left((-x_+(t))^2 - (-x_-(t))^2\right) + ... \tag{13}$$

We can insert the solution from eq.(11) into eq.(13) to expand this further. We will also define $\hat{E} = \frac{eE_0}{C_+\omega x_f}$ and $\delta = \frac{C_+}{C_-}$ for notational convenience

$$E_f(t) \approx \frac{ke}{x_f^2}\left(-2\hat{E}\cos(\omega t) - 2\hat{E}\delta\cos(\omega t) + 3\hat{E}^2\cos^2(\omega t) - 3\hat{E}^2\delta^2\cos^2(\omega t)\right) + ...$$

$$= \frac{ke}{x_f^2}\left(-2\hat{E}(1 + \delta)\cos(\omega t) + 3\hat{E}^2(1 - \delta^2)\cos^2(\omega t)\right) + ... \tag{14}$$

If the particles experience the same drag such that $\delta = 1$, this expression only has odd powers of $\cos(\omega t)$, this is shown in figure 4. If $\delta \neq 1$ the expression contains both odd and even terms, this is shown in figure 5.

Since the odd terms average out to zero but the even terms do not, the average electric fields have a finite value if $\delta \neq 1$.
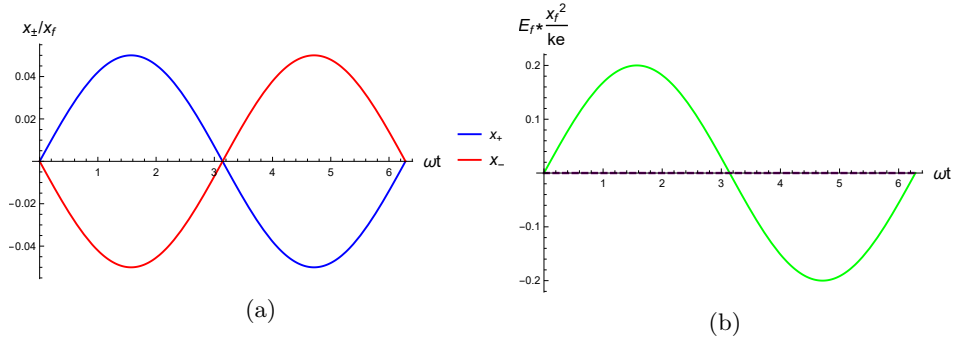
Figure 4: (a) The positions of the cation x_+ (blue) and anion x_- (red) as a function of time for equal mobilities ($\delta = 1$). (b) The perturbation of the electric field far from the ions (E_f) as a function of time (green) and the average field over one oscillation (purple). In both (a) and (b), $\hat{E} = 0.05$.
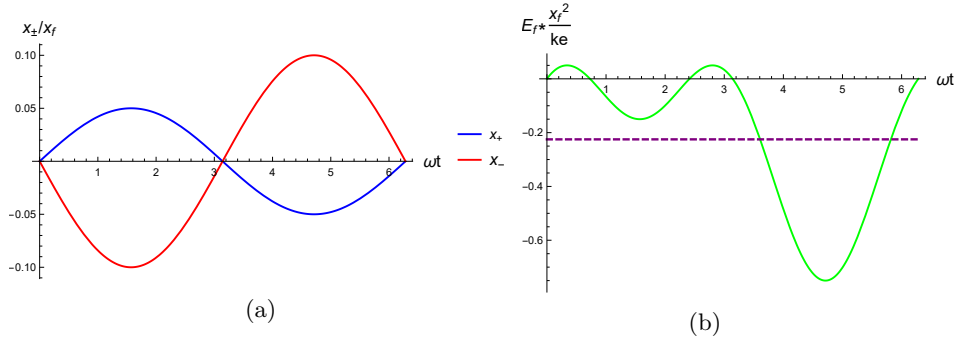
Figure 5: (a) The positions of the cation x_+ (blue) and anion x_- (red) as a function of time for unequal mobilities ($\delta = 2$). (b) The perturbation of the electric field far from the ions (E_f) as a function of time (green) and the average field over one oscillation (purple). In both (a) and (b) $\hat{E} = 0.05$.

10

2.3 Pumping

In section 1 we mentioned that ACEO can be used to pump fluids. In this section, we will provide a brief description of how this could be achieved. Methods of pumping have been proposed before [4][5]. The electrodes used in these pumps are different from what we will be studying. The electrodes are placed in the same plane, such that the electric field between them is parallel to the surface. In both [4] and [5] the flow is caused by asymmetries in the electrodes. We studied asymmetric electrolytes, so the same principles do not apply. Instead, we will try to give an intuition of how pumping can be achieved by using the AREF as a driving field for regular (DC) electroosmosis. This would be done in a channel between the two electrodes as shown in figure 6.

We will assume the AREF has fully formed and is given by:
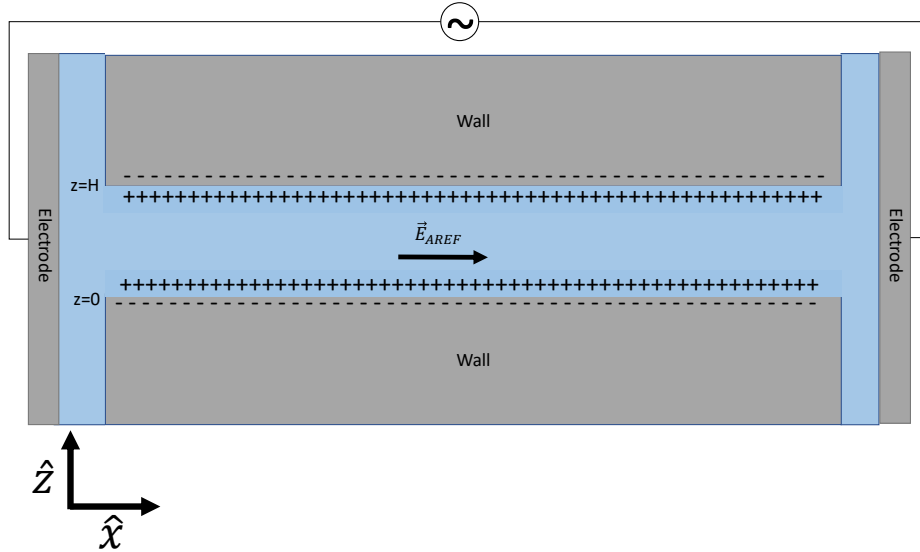
Figure 6: An electrolyte in a channel between two planar electrodes. The walls of the channel are charged, such that an EDL forms on their surface. an oscillating potential is applied to the electrodes, causing an AREF to form.

$$\vec{E}_{AREF} = \begin{pmatrix} E_x \\ 0 \\ 0 \end{pmatrix}. \tag{15}$$

We approximated the oscillating field by its average value, and we will assume it is constant in the channel. The AREF will push on the EDLs that have formed on the channel wall and drag the fluid along. We can use the stationary stokes equation to calculate the flow field [10]:

$$\eta \nabla^2 \vec{u}(x,y,z) = e(z_+ n_+ + z_- n_-)\vec{E}_{AREF} = \epsilon \left(\nabla^2 \phi(x,y,z)\right) \vec{E}_{AREF}. \tag{16}$$

Here, η is the viscosity of the solvent, and $\vec{u}(x, y, z)$ is the flow velocity. We assume that ϕ consists of the AREF on one hand, and the EDLs on the channel walls on the other hand. We can write this as:

$$\phi(x, y, z) = E_x x + \phi_c(y, z). \tag{17}$$

Here, $E_x x$ is the potential that gives rise to the AREF, and $\phi_c(y, z)$ is that caused by the EDLs on the channel walls.

We can simplify eq.(16) by making use of symmetries and making some assumptions. Since there is translational invariance in the $\hat{y}$ direction, $u_y = 0$ and $\frac{\partial^2 \phi}{\partial y^2} = \frac{\partial^2 u}{\partial y^2} = 0$. Also, $u_z = 0$ since the $\hat{z}$ direction is blocked by the channel walls. Since both u_y and u_z are 0, u only has an $\hat{x}$ component. We assumed the AREF was a constant field in the channel, so $\frac{\partial^2 \phi}{\partial x^2} = 0$. Since both $\frac{\partial^2 \phi}{\partial x^2} = 0$ and $\frac{\partial^2 \phi}{\partial y^2} = 0$, $\nabla^2 \phi = \frac{\partial^2 \phi_c}{\partial z^2}$. Because $\epsilon \left(\frac{\partial^2 \phi_c(z)}{\partial z^2} \right) E_x$ is independent of x there is no reason why u should change with x, so we assume $\frac{\partial^2 u_x}{\partial x^2} = 0$.

With all of these simplifications, eq.(16) becomes:

$$\frac{\partial^2 u_x(z)}{\partial z^2} = \frac{\epsilon E_x}{\eta} \left(\frac{\partial^2 \phi_c(z)}{\partial z^2} \right) \tag{18}$$

If we now assume a no-slip boundary condition on the channel walls ($u_x(0) = u_x(H) = 0$), we can integrate eq:(18) to give:

$$u_x(z) = \frac{\epsilon}{\eta} E_x (\phi_c(z) - \phi_c(0)). \tag{19}$$

This flow depends linearly on the strength of the AREF.

2.4   Poisson-Nernst-Planck equations

Now that we have introduced the important concepts, we can move on to describing the system shown in figure 1. We want to study the behaviour of the ions subject to a time-dependent potential, the equations that govern this behaviour are the Poisson-Nernst-Planck (PNP) equations [11]. The first of the PNP equations is the Poisson equation [12]:

$$- \epsilon \nabla^2 \phi = \rho. \tag{1}$$

which relates the Laplacian of the electric potential ϕ to the charge density ρ. Using the fact that our system is translationally invariant in the y and z directions, we can rewrite the Poisson equation as:

$$- \epsilon \frac{\partial^2 \phi}{\partial x^2}(t, x) = e(z_+ n_+(t, x) + z_- n_-(t, x)). \tag{20}$$

The only differences with eq.(1) are z_+ and z_-, these are the valencies of the cations and anions respectively, which can now take values other than ± 1.

12

The second of the PNP equations is the Nernst-Planck equation [13]:

$$j_\pm(t,x) = -D_\pm\left(\frac{\partial n_\pm}{\partial x}(t,x) + \frac{ez_\pm}{k_BT}n_\pm(t,x)\frac{\partial \phi}{\partial x}(t,x)\right), \qquad (21)$$

where $D_\pm$ is the diffusion constant for the cations/anions, and $j_\pm$ is the cation/anion flux. The first term in eq.(21) accounts for Fickian diffusive transport. It describes the tendency of particles to move from regions of high concentration to regions of low concentration. The second term in eq.(21) accounts for Ohmic electric transport. This describes the forces felt by the ions due to the electric fields in the system. Note that we have implicitly assumed that the response of the flux is linear in the gradients of the potential and concentrations.
Finally, the system must obey conservation of mass and charge. This is described by a continuity equation [14]:

$$\frac{\partial n_\pm}{\partial t}(t,x) = -\frac{\partial j_\pm}{\partial x}(t,x), \qquad (22)$$

which describes the conservation of the ions. Eq.(22) can be expanded to include chemical reactions, but we assume that these do not occur.

To get a closed set of equations for $n_\pm(x,t)$, $\phi(x,t)$, and $j_\pm(x,t)$, we need to define the initial and boundary conditions of the system. We choose the initial conditions for $n_\pm$ such that the concentrations are homogeneous and the system is charge neutral everywhere:

$$n_\pm(t=0,x) = n_{s\pm} \equiv \frac{n_0}{1\pm\gamma}, \qquad (23)$$

where n_0 is a constant concentration that will be scaled out later, and $\gamma = \frac{z_+ + z_-}{z_+ - z_-}$ is a factor that determines the difference in valence between the cations and anions (see section 3).
For $j_\pm$ we use the 'blocking electrode' boundary condition, which states that there can be no transport through the electrodes. This means we ignore any chemical reactions between the electrodes and the electrolyte,

$$j_\pm(t,x=0) = j_\pm(t,x=L) = 0. \qquad (24)$$

Finally, at any given time the electric potential at the electrodes is set. We use an AC potential

$$\phi(t,x=0) = -\phi(t,x=L) = \phi_0\sin(\omega t), \qquad (25)$$

where ϕ_0 and ω are the amplitude and frequency of the oscillation, respectively. They are system parameters that can be varied.

3 Methods

The PNP equations form a closed set, but their non-linear nature makes them difficult to solve without making some simplifying assumptions. We get around that difficulty by solving the equations numerically. To that end, it is convenient to first make the equations dimensionless. The way we have done this is similar to the methods used by Amrei et al.[8]. First, we define a diffusivity magnitude $D = \frac{2D_+D_-}{D_++D_-}$ and a dimensionless diffusivity difference $\beta = \frac{D_+-D_-}{D_++D_-}$. Now we can write the two diffusion constants as:

$$D_\pm = \frac{D}{1 \mp \beta}. \tag{26}$$

In a similar fashion, we define the valence magnitude $z = \frac{1}{2}(z_+ - z_-)$ and valence difference $\gamma = \frac{z_++z_-}{z_+-z_-}$, it should be noted that $z_+ > 0$ and $z_- < 0$. We can now write:

$$z_\pm = (\gamma \pm 1)z. \tag{27}$$

The desired valence and diffusivity differences can now be set by choosing the right values of γ and β. Setting either parameter to zero corresponds to having equal valences and diffusivities respectively. Typically, $z_\pm$ take integer values from ± 1 to ± 3. This puts typical values of γ between $-\frac{1}{2}$ and $\frac{1}{2}$. Typical values of $D_\pm$ range from 0.5 to 2 nm^2/ns. This gives the typical range of β between -0.6 and 0.6. Initially, we set $\gamma = 0$, but it is left in the equations to allow for different valencies later on.

We make the ion concentrations dimensionless by scaling them to the constant in their initial value, which we called n_0. This gives a dimensionless density $\tilde{n}_\pm = \frac{n_\pm}{n_0}$. We scale ϕ with the thermal energy, giving us $\tilde{\phi} = \frac{\phi z e}{k_B T}$. The scale we use for distances is the Debye length $\kappa^{-1} = \sqrt{\frac{\epsilon k_B T}{2e^2 z^2 n_0}}$, this gives $\tilde{x} = x\kappa$ as well as $\tilde{L} = L\kappa$. Our definition of κ may look slightly different from the normal definition, but it is equivalent. We prove that the definitions are equivalent in section 6.1.

In the scaling for the time we deviate somewhat from Amrei et al. Whereas they define $\tilde{t} = \kappa^2 D t$, we scale the time by the so-called RC time $\tau_{RC} = \frac{L}{D_{RC}\kappa}$ where $D_{RC} = \frac{D_++D_-}{2} = \frac{D}{1-\beta^2}$. Using this to scale the time gives us:

$$\tilde{t} = t/\tau_{RC} = t\frac{\kappa D_{RC}}{L} = t\frac{\kappa^2 D}{\tilde{L}(1-\beta^2)}. \tag{28}$$

We also scale the frequency by the inverse RC-time: $\tilde{\omega} = \omega \tau_{RC}$

With all the dimensionless variables, we can now construct the dimensionless PNP equations. For notational convenience, we leave out the tildes in the remainder of this section.

$$-\frac{\partial^2 \phi}{\partial x^2} = \frac{1}{2}((1+\gamma)n_+ - (1-\gamma)n_-); \tag{29}$$

$$\frac{\partial n_\pm}{\partial t} = -L(1-\beta^2)\frac{\partial j_\pm}{\partial x}; \tag{30}$$

$$j_\pm = -\frac{1}{1 \mp \beta}\left(\frac{\partial n_\pm}{\partial x} \pm (1 \pm \gamma)n_\pm \frac{\partial \phi}{\partial x}\right). \tag{31}$$

In this section we will discuss the numerical methods we used to solve the PNP equations. We first need to discretise the system. To do this we divide the space between the electrodes into a grid of N points with constant distance $\Delta x = \frac{L}{N}$ between them. This sounds simple, but there is one important point to consider: are the electrodes on grid points or between them? Because it simplifies the way ϕ and j are calculated, we choose to place the electrodes between points. This means the first point is just to the right of the electrode at $x = 0$, and the Nth point is just to the left of the electrode at $x = L$. The x-coordinate of point k is $x_k = (k - \frac{1}{2})\Delta x$ (see figure 7). For example $x_1 = \frac{\Delta x}{2} = \frac{L}{2N}$. We also define a time step of duration Δt, so that the time at step i is $t_i = i\Delta t$.
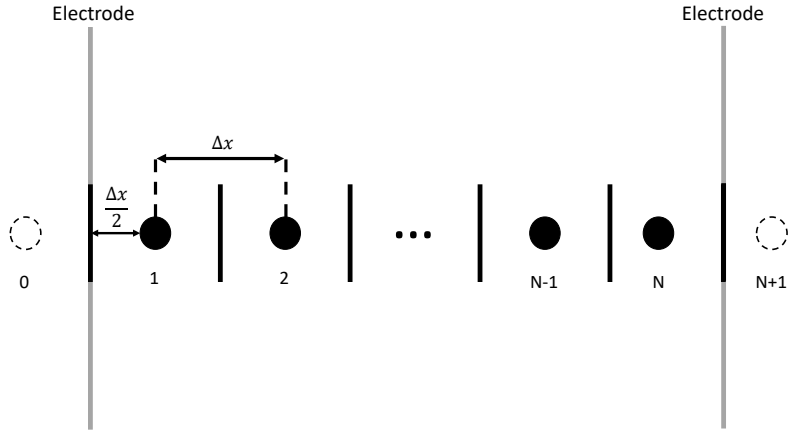
Figure 7: A schematic representation of the grid used for discretisation. Dots represent grid points on which we define the variables ϕ and $n_\pm$, the lines represent the halfway point between two grid points on which we define $j_\pm$ and the gradients $\frac{\partial \phi}{\partial x}$ and $\frac{\partial n_\pm}{\partial x}$. The point k is at position $x_k = (k - \frac{1}{2})\Delta x$. $k \in 1, ..., N$.

Since n_+ and n_- are already determined for the initial time step ($t = 0$), we first calculate the electric potential for that same step. To do this we begin by discretising eq.(29) using the finite difference method. Specifically, we use the central difference method to express the second derivative of ϕ at one point in terms of the value of ϕ at the surrounding points. From now on, we use the superscript i to indicate a point in time and the subscript k to indicate a point in space.

$$\left(\frac{\partial^2 \phi}{\partial x^2}\right)_k^i = \frac{\phi_{k+1}^i - 2\phi_k^i + \phi_{k-1}^i}{\Delta x^2}, \tag{32}$$

for $1 \leq k \leq N - 1$ with N the number of grid points between the electrodes. Thanks to eqs.(29) and (23), the left hand side of eq.(32) is already known. With a bit of work, we can rewrite eq.(32) as a matrix-vector equation:

$$-\frac{1}{2}\mathbf{B}((1+\gamma)\vec{n}_+^i - (1-\gamma)\vec{n}_-^i) + \vec{C} = \mathbf{D}\vec{\phi}^i \tag{33}$$

where $\vec{n}_\pm^i$ and $\vec{\phi}^i$ are vectors containing the values of $n_\pm$ and ϕ at each point in space at time t_i. That is: the k-th component of $\vec{\phi}^i$ is ϕ_k^i. Here, $\mathbf{B}$ and $\mathbf{D}$ are matrices, and $\vec{C}$ is a vector. We will derive these in appendix 6.3. Once we know all of these matrices, we can use any matrix inversion program to calculate $\vec{\phi}^i$:

$$\vec{\phi}^i = -\frac{1}{2}\mathbf{D}^{-1}\mathbf{B}((1+\gamma)\vec{n}_+^i - (1-\gamma)\vec{n}_-^i) + \mathbf{D}^{-1}\vec{C}. \tag{34}$$

We used the "mldivide" command built in to MATLAB [15].

Once we have ϕ and $n_\pm$ for a given time step, we can calculate $j_\pm$ from eq.(31). Because $j_\pm$ is a gradient, it is technically defined between the grid points. By simply applying a first-order finite difference method to eq.(31), we find that the ion flow between two points is given by:

$$j_{\pm k+1/2}^i = -\frac{1}{1 \mp \beta}\left(\frac{n_{\pm k+1}^i - n_{\pm k}^i}{\Delta x} \pm (1 \pm \gamma)n_{\pm k+1}^i\frac{\phi_{k+1}^i - \phi_k^i}{\Delta x}\right). \tag{35}$$

The boundary conditions become $j_{\pm 1/2}^i = j_{\pm N+1/2}^i = 0$. Once $n_\pm$, ϕ and $j_\pm$ have all been calculated for a given time step, we can calculate $n_\pm$ for the next time step. We discretise eq.(30) by using the forward difference method on the left hand side, and the central difference method on the right hand side, this gives us:

$$n_{\pm k}^{i+1} = n_{\pm k}^i + L(1-\beta^2)\frac{\Delta t}{\Delta x}(j_{\pm k-1/2}^i - j_{\pm k+1/2}^i). \tag{36}$$

We then repeat this process for as many time steps as we need. Before we start measurements, we need to let the program run for a while to get rid of the transients. We found that a run time of $t_{run} = 125\tau_{RC}$ was sufficient even at high frequencies. We took our measurements over the last period ($\frac{2\pi}{\omega}$) of this run time. In the very low frequency domain, this run time would be shorter than one period, so we chose a run time of exactly three periods.

A small issue with our methods is that the methods used to calculate $n_\pm$ are only stable if $\frac{2L}{1-\beta^2}\frac{\Delta t}{\Delta x^2} < \frac{1}{2}$ [16]. If this condition is not met, the error caused by the fact that we use a first order approximation will keep growing with each iteration and eventually diverge. Because the electric double layer plays an important role in this system, we want to model it properly. This limits how large our space step size (Δx) can be, as we want at least ten grid points within the size of the double layer (κ^{-1}). To accommodate, we have to keep the time step size (Δt) quite small. Unfortunately, this increases the number of time steps needed to properly model the system. We decided to use the step sizes $\Delta x = 0.1$ and $\Delta t = 0.00005$, we keep these the same in all results to avoid confusion.

4 Results

4.1 Electric double layer

We measure ϕ, $n_\pm$, and $j_\pm$ as a function of space and time. To get an intuition into what happens we will show a few snapshots of the electric potential and the charge concentration ($\tilde{n} = z_+\tilde{n}_+ - z_-\tilde{n}_-$) as a function of position in figures 8 and 9. In both figures, $\frac{D_+}{D_-} = 2$ and $\frac{z_+}{z_-} = 1$.

(a)   (b)
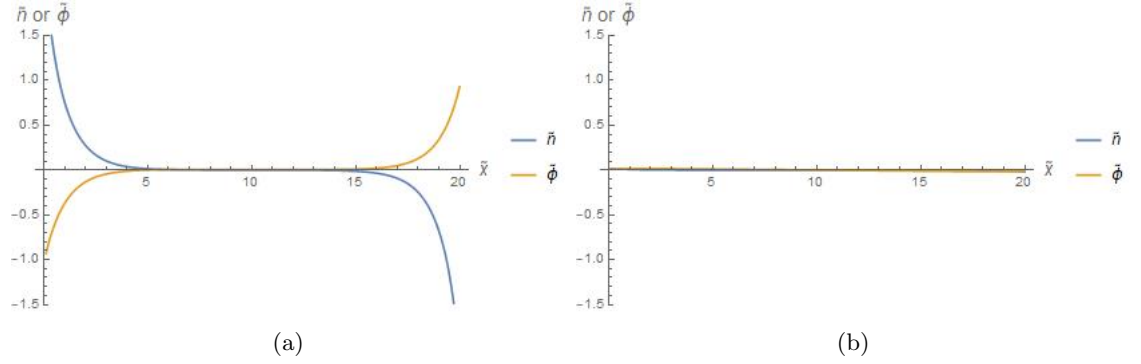
Figure 8: Snapshots of the electric potential $\tilde{\phi}$ and charge concentration $\tilde{n}$ as a function of position for $\tilde{\omega} \approx 0.05$, $\frac{D_+}{D_-} = 2$, $\frac{z_+}{z_-} = 1$, $\tilde{\phi}_0 = 1$, and $\tilde{L} = 20$. The snapshots were taken at the time where (a) $|\tilde{\phi}(t,0)| = \tilde{\phi}_0$ and (b) $|\tilde{\phi}(t,0)| = 0$.

(a)   (b)
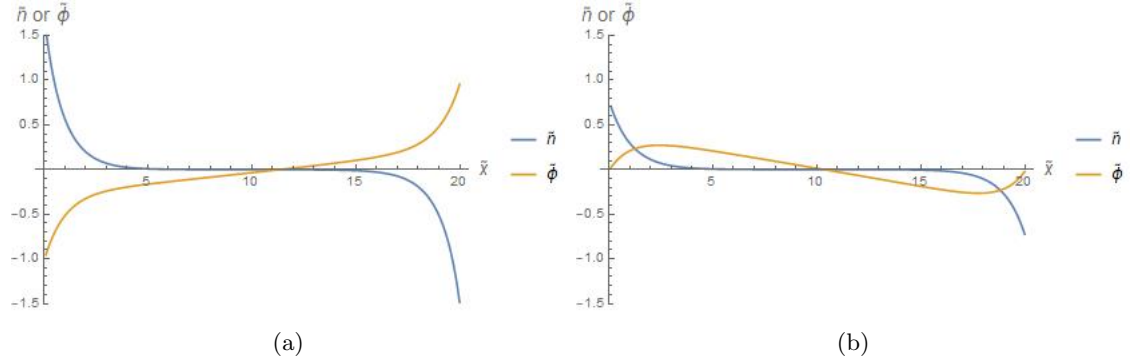
Figure 9: Snapshots of the electric potential and charge concentration as a function of position for $\tilde{\omega} \approx 1$, $\frac{D_+}{D_-} = 2$, $\frac{z_+}{z_-} = 1$, $\tilde{\phi}_0 = 1$, and $\tilde{L} = 20$. The snapshots were taken at the time where (a) $|\tilde{\phi}(t,0)| = \tilde{\phi}_0$ and (b) $|\tilde{\phi}(t,0)| = 0$.

Figure 8 shows that for low frequencies ($\tilde{\omega} \approx 0.05$), the oscillations of ϕ and n are synchronised, and the EDL can form properly during every period. Because of this, the solution at any time matches the steady-state solution for a

non-oscillating system with the electrode potential kept at $\pm\phi_0 \sin(\omega t)$. Figure 9 shows that for higher frequencies ($\tilde{\omega} \approx 1$), ϕ and n are no longer synchronised. Since the positive ions can move faster than the negative ones, it takes less time for the positive EDL to form than the negative one. If the applied frequency is low, there is enough time for both types of ions to form their EDL, and there is no asymmetry. As the frequency increases, the negative ions will increasingly lag behind and fail to form a complete EDL. When this happens, the potential is no longer symmetric (see figure 9(a)). When we take the average of this asymmetric potential over one period of the driving oscillation, we find a non-zero average potential.

4.2 Average central potential

The first thing we will investigate is the electric potential at the center of the system averaged over one period of the oscillation defined as:

$$\langle \tilde{\phi}_{mid} \rangle = \frac{\tilde{\omega}}{2\pi} \int_{t_{run} - \frac{2\pi}{\omega}}^{t_{run}} \tilde{\phi}(t, \frac{L}{2}) dt \tag{37}$$

We could just as well have replaced $\tilde{\phi}(t, \frac{L}{2})$ the spatial integral over the entire system, but the results are similar, so we restrict ourselves to the center of the system. First, we kept the system size constant and varied ω for different values of $\tilde{\phi}_0$. The other system parameters were as follows: $\tilde{L} = 15$, $d\tilde{x} = 0.1$, and $\beta = \frac{1}{3}$ which means $\frac{D_+}{D_-} = 2$. We run the program for long enough so that the system can reach its steady state, and then average the potential over one period.
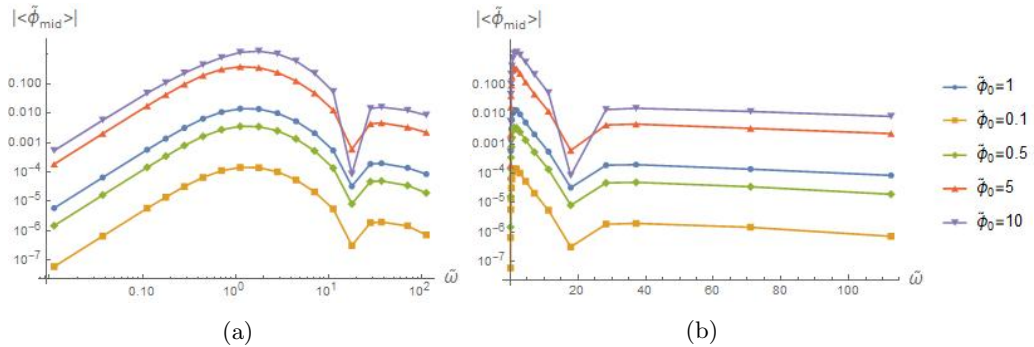
Figure 10: The absolute value of late-time period-average $|\langle \tilde{\phi}_{mid} \rangle|$ as a function of the driving frequency $\tilde{\omega}$ for several values of the driving amplitude $\tilde{\phi}_0$ on (a) a double logarithmic scale, and (b) a logarithmic scale. System parameters are: $\tilde{L} = 15$, $\gamma = 0$, and $\beta = 1/3$.

In figure 10 we plot the absolute value of the time-averaged potential $\langle \tilde{\phi}(x = \frac{L}{2}) \rangle$ at the center of the system as a function of the driving frequency $\tilde{\omega}$. In (a) we
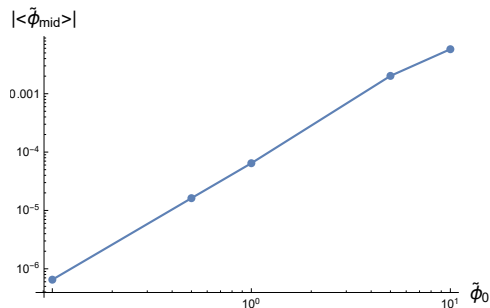
Figure 11: The absolute value of late-time period-average $|\langle\tilde{\phi}_{mid}\rangle|$ as a function of the driving amplitude $\tilde{\phi}_0$ on a double logarithmic scale. The slope is approximately 2. System parameters are: $\tilde{\omega} \approx 0.04$, $\tilde{L} = 15$, $\gamma = 0$, and $\beta = 1/3$.

plotted the data on a log-log scale, and in (b) we plotted it on a lin-log scale. We can extract some of the behaviour of $\langle\phi\rangle$ by looking at the parts of these graphs that are (approximately) linear in the relevant scales. In the left half of figure 10, one can see that there is a linear part at the very lowest values of ω. Using a linear model fit we found that the slope of this line converges to 2 for low frequencies. This suggests that for $\tilde{\omega} \ll 1$, $|\langle\phi_{mid}\rangle| \propto \omega^2$.

Looking at individual points on the different graphs in figure 10, we can see that the average potential at the center seems to scale with the square of the applied potential. We confirm this by plotting the average central potential as a function of the driving amplitude in figure 11. Here we once again find a slope of approximately 2 in the double logarithmic scale, which confirms that $|\langle\tilde{\phi}_{mid}\rangle| \propto \tilde{\phi}_0^2$. Our finding that $|\langle\tilde{\phi}_{mid}\rangle| \propto \tilde{\phi}_0^2$ is consistent with results found by Amrei et al. [6].

Another interesting feature is the apparent local minimum at $\tilde{\omega} \approx 20$. It looks like there is a discontinuity in the graph, but this is a side effect of plotting in log scales. Figure 12 shows the same $\tilde{\phi}_0 = 1$ data as figure 10, but in linear scale. The 'minimum' seen in figure 10 is actually a zero-point where the sign of the potential changes. We can clearly see from figure 10 that the frequency at the the zero-point does not depend on the value of ϕ_0.

To investigate further, we fixed $\phi_0 = 1$ and varied the length of the system. Again, we plot the data in both log-log and lin-log scales. Figure 13 shows many of the same features seen in figure 10. For the very low values of ω, we once again see a slope of 2 in the double logarithmic scale. The location of the minimum (ω_{min}) does depend on the length of the system. We can plot the location of the minimum (ω_{min}) as a function of the system size to see how they are related.
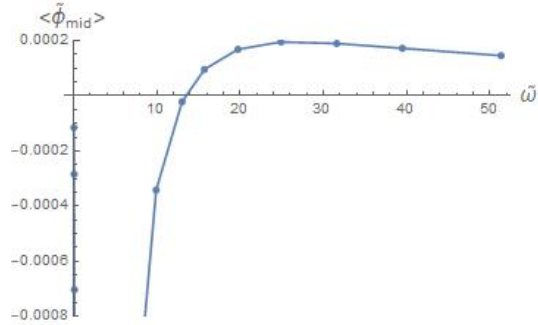
Figure 12: The late-time period-average $\langle \tilde{\phi}_{mid} \rangle$ as a function of the driving frequency $\tilde{\omega}$ in linear scale. System parameters: $\tilde{L} = 15$, $\phi_0 = 1$, $\beta = 1/3$, $\gamma = 0$.
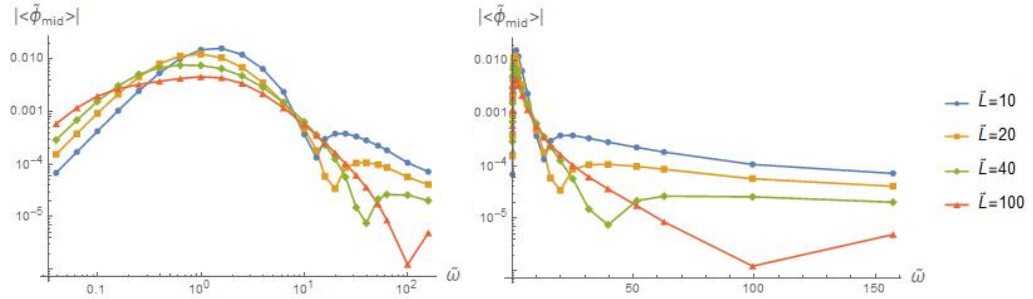
Figure 13: The absolute value of late-time period-average $|\langle \tilde{\phi}_{mid} \rangle|$ as a function of the driving frequency $\tilde{\omega}$ for several values of the system size $\tilde{L}$ on (a) a double logarithmic scale, and (b) a logarithmic scale. System parameters are: $\tilde{\phi}_0 = 1$, $\gamma = 0$, and $\beta = 1/3$.

Figure 14 shows the position of the minimum as a function of the system length. We used different units in the plot on the right of figure 14. The units used in the plot on the right can be interpreted as the time it takes an ion to diffuse a distance κ^{-1}. It seems clear that there is a linear connection between ω_{min} and L. The slope of the left plot is approximately 1.

The reason that there would be a zero point here is that this is the frequency at which neither the positive nor the negative ions have enough time to form an EDL. This means no asymmetry is introduced into the system, so $\langle \phi_{mid} \rangle$ will be zero. It is unclear why the potential changes sign for even higher frequencies.
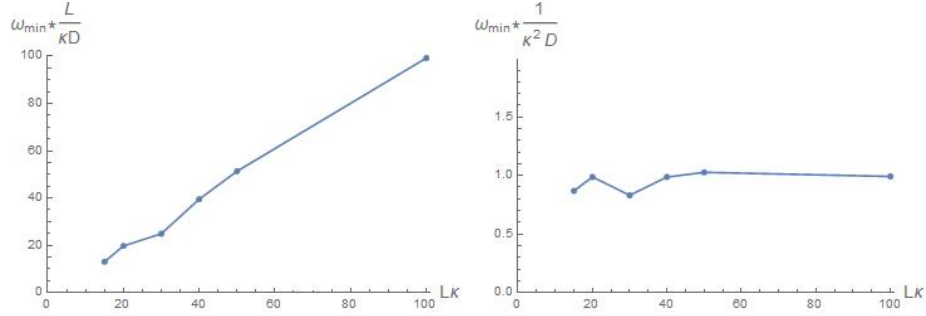
Figure 14: (left) The location of the minimum found in figures 10 and 13 as a function of the system size. (right) The same data, but expressed in different units of ω. The units used in the right plot can be interpreted as the time it takes for an ion to diffuse a distance κ^{-1}. System parameters: $\tilde{\phi}_0 = 1$, $\beta = 1/3$, $\gamma = 0$.

4.3 Fourier analysis

In order to see what happens when the sign changes, we also look at the value of ϕ_{mid} as a function of time for several values of ω. Figure 15 shows that for frequencies near the maximum in figures 10 and 13(shown in green), the frequency at the center is double that of the frequency at the electrodes. At the minimum (shown in red), the frequency halves and becomes equal to that at the electrodes. Another perhaps more interesting feature is that we see some smaller peaks and valleys in the very low frequencies(shown in blue). These suggest that there might be a higher Fourier mode that only becomes relevant at these low frequencies.

To investigate this low frequency Fourier mode, we use a discrete Fourier transform on the data shown in figure 15. This transformation takes the form:

$$\hat{\phi}(\omega_m) = \sum_{n=0}^{N-1} \tilde{\phi}_{mid}(t_n) e^{-i\frac{2\pi}{N}nm}. \tag{38}$$

Here, $t_n = n\Delta t$, $\omega_m = m\tilde{\omega}$, and we defined $\hat{\phi}(\omega)$ as the Fourier transform of $\phi_{mid}(t)$. We used a subscript n to indicate the time step to avoid confusion with the imaginary number $i = \sqrt{-1}$. In the convention we used, the inverse Fourier transform takes the form:

$$\tilde{\phi}_{mid}(t_n) = \frac{1}{N} \sum_{m=0}^{N-1} \hat{\phi}(\omega_m) e^{i\frac{2\pi}{N}nm}. \tag{39}$$

We plot the Fourier transform for the same three driving frequencies used in figure 15. The colours in figure 16 are the same as those in figure 15.

(a)

(b)

(c)
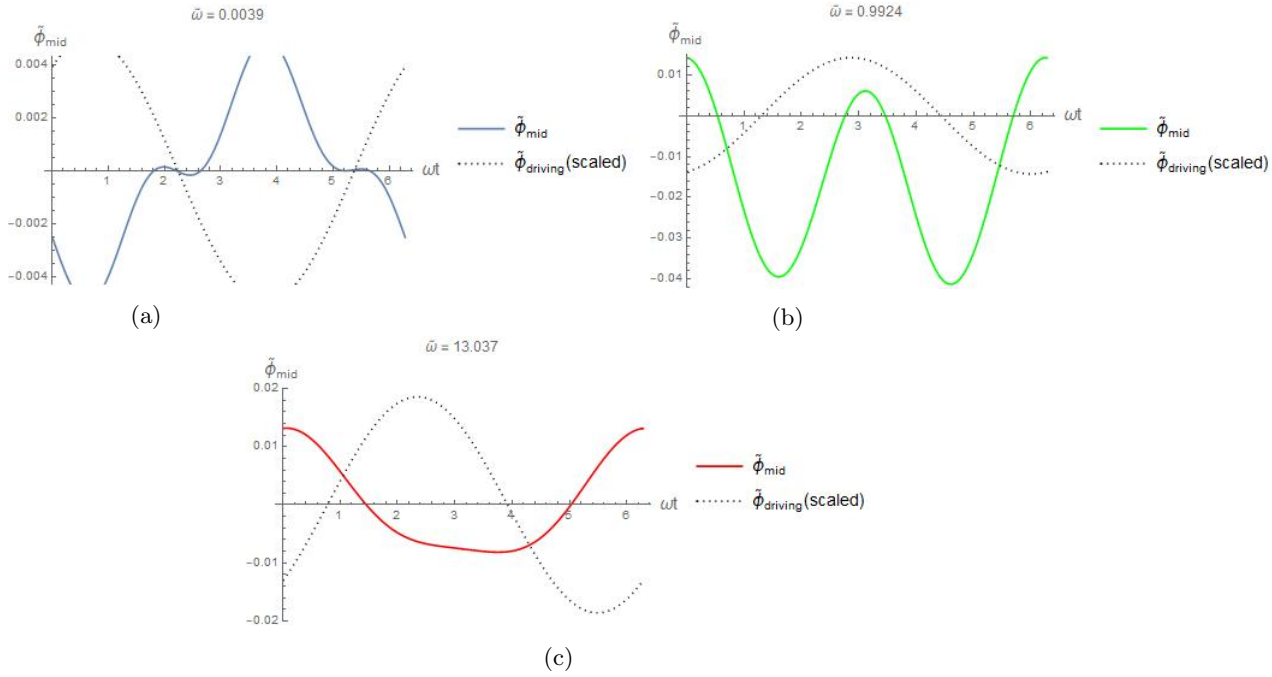
Figure 15: The electric potential at the center of the system as a function of time over one period of the oscillation. (a) Shows a very low frequency, (b) and (c) show the frequencies at the maximum and minimum in figures 10 and 13 respectively. The dotted lines show the applied potential at the electrodes scaled to the amplitude of ϕ_{mid}. System parameters: $\tilde{L} = 10$, $\tilde{\phi}_0 = 1$, $\beta = 1/3$, $\gamma = 0$.

(a)

(b)

(c)
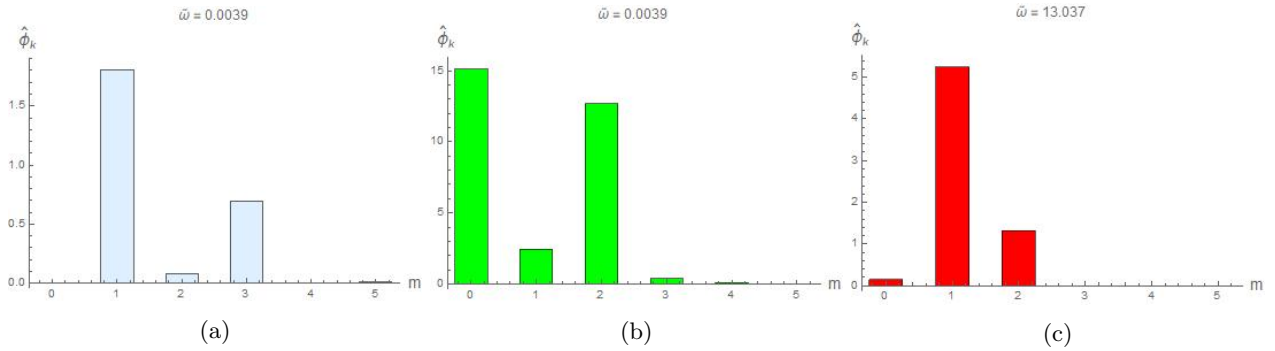
Figure 16: The Fourier transform of the electric potentials shown in figure 15. We only show $m = 0$ through $m = 5$, as there are no other peaks beyond those displayed.

Figure 16 shows the Fourier transforms of the three plots in figure 15. We zoomed in on the $m = 0$ through $m = 5$ modes as this is where the interesting behaviour lies. In the low frequency domain (a) we see that there are two important Fourier coefficients: $\hat{\phi}_1$ and $\hat{\phi}_3$, with $\hat{\phi}_1$ being the most important. This can be related back to figure 15(a) by noting that there, we see an oscillation at the driving frequency with a smaller oscillation mixed in. Similarly at the RC frequency ($\tilde{\omega} \approx 1$) in figure 16(b) we see peaks at $\hat{\phi}_0$ and $\hat{\phi}_2$. This corresponds to an oscillation at twice the driving frequency with a constant offset. Looking back at figure 15(b) we see exactly this behaviour. Finally, figure 16(c) shows a large peak at $\hat{\phi}_1$ and a smaller peak at $\hat{\phi}_2$ for high frequencies. This corresponds to the imperfect oscillation at the driving frequency we see in figure 15(c). As mentioned in section 2.2 the odd Fourier modes do not give rise to a finite average potential, while the even modes do. Figure 16 shows that the even modes are much more pronounced at the maximum than at the other frequencies.

4.4 Valencies and diffusion constants

Next, we wish to see if giving the ions different valencies instead of different diffusion coefficients yields the same results. To this end we make a copy of figure 13, but set $\frac{D_+}{D_-} = 1$ and $\frac{z_+}{z_-} = 2$. The model does not need to be adapted for this change, as we allowed for different valencies from the beginning. Using the definitions in section 3, we can see that setting $\frac{z_+}{z_1} = 2$ is equivalent to setting $\gamma = 1/3$. Eq.(23) guarantees that the system is charge neutral regardless of the relative charges of the ions. We do not need a large variety of lengths as we have already shown the interesting length-dependent features, so we only plot the $\kappa L = 20$ and $\kappa L = 50$ versions in case a feature we have not yet seen appears.

Figure 17 is similar to figure 13 in the high frequency domain. We still see the zero points close to $\tilde{\omega} = \tilde{L}$. For the frequencies below $\tilde{\omega} = 1$, something interesting happens. Rather than decay to zero, the average potential stays almost constant. Furthermore, the potential is almost identical for the two different system sizes.

To understand why there is a finite potential at very low frequencies, we make some snapshots of the potential $\tilde{\phi}(t, x)$ and charge density $n(t, x)$ as a function of x for two different values of t.
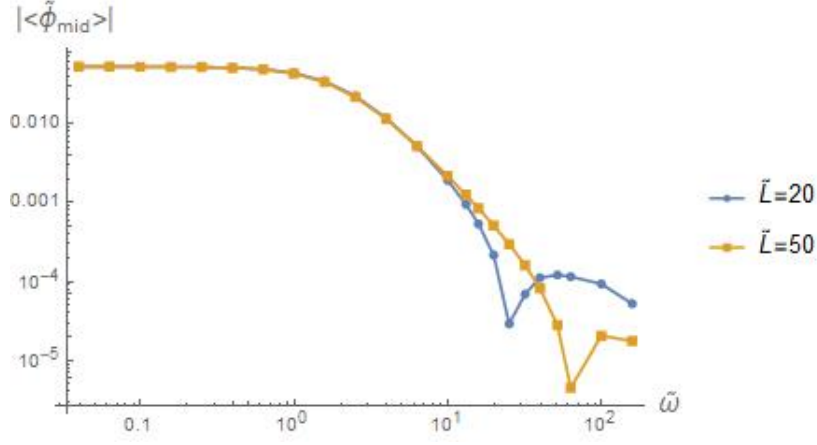
Figure 17: The absolute value of late-time period-average $|\langle \tilde{\phi}_{mid} \rangle|$ as a function of the driving frequency $\tilde{\omega}$ and system size $\tilde{L}$. System parameters: $\tilde{\phi}_0 = 1$, $\frac{D_+}{D_-} = 1$, $\frac{z_+}{z_-} = 2$.

(a)   (b)
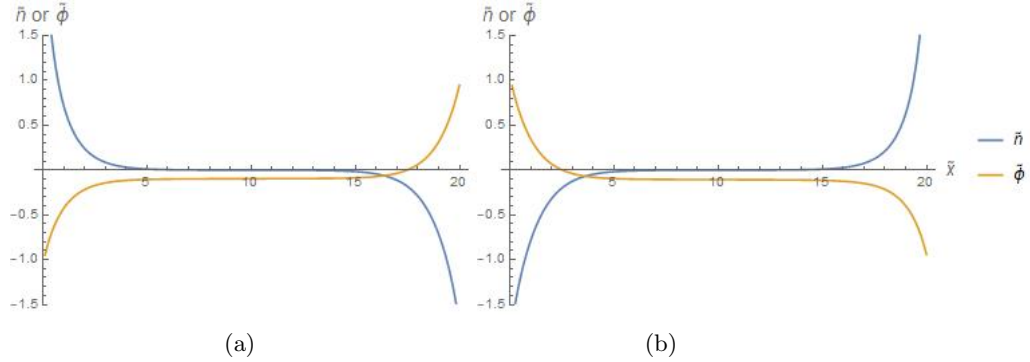
Figure 18: Snapshots of ϕ and n as a function of space at a time where (a) $\tilde{\phi}_0 \sin \omega t = \tilde{\phi}_0$ and (b) $\tilde{\phi}_0 \sin \omega t = -\tilde{\phi}_0$ for $\tilde{\omega} = 0.0626131$. The potential near the center takes the same finite value at both times. System parameters: $\tilde{L} = 20$, $\tilde{\phi}_0 = 1$, $\beta = 0$, $\gamma = 1/3$.

Figure 18 shows the potential and charge density as a function of space at the times where $\tilde{\phi}_0 \sin \omega t = \tilde{\phi}_0$ and $\tilde{\phi}_0 \sin \omega t = -\tilde{\phi}_0$. In both cases, the potential around the center of the system takes a small negative value. We also plot the central potential as a function of time in figure 19. Figure 19 shows that the potential at the center is always negative and oscillates between zero and the values shown in figure 18. The way the EDLs form at low frequencies when both types of ions have enough time is already asymmetrical. This will cause the average potential to remain finite as $\tilde{\omega} \to 0$.
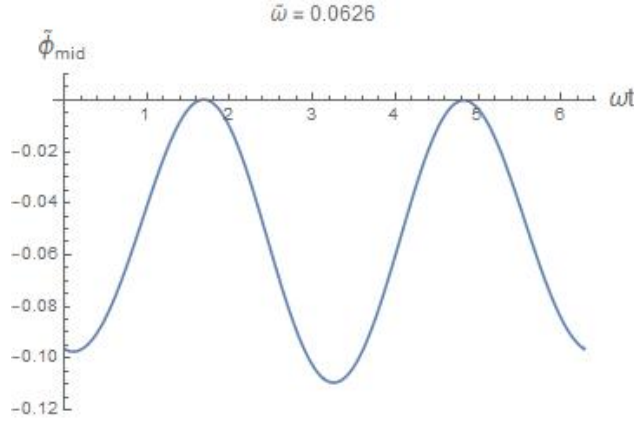
Figure 19: The central potential ϕ_{mid} as a function of time over one period of the oscillation for a system with different valencies. System parameters: $\tilde{\omega} = 0.0626$, $=20$, $_0 = 1, \beta = 0, \gamma = 1/3$

We have now examined both the case of different diffusion coefficients with equal valencies and the case of equal diffusion constants with different valencies. We now ask ourselves a few questions: what happens if we further increase the values of $\frac{D_+}{D_-}$ and $\frac{z_+}{z_-}$, and what happens if we have different diffusion constants and different valencies simultaneously? Starting with the first question, we run the program again with $\frac{D_+}{D_-} = 3$ ($\beta = \frac{1}{2}$) and $\frac{z_+}{z_-} = 1$ ($\gamma = 0$). This is shown in figure 20
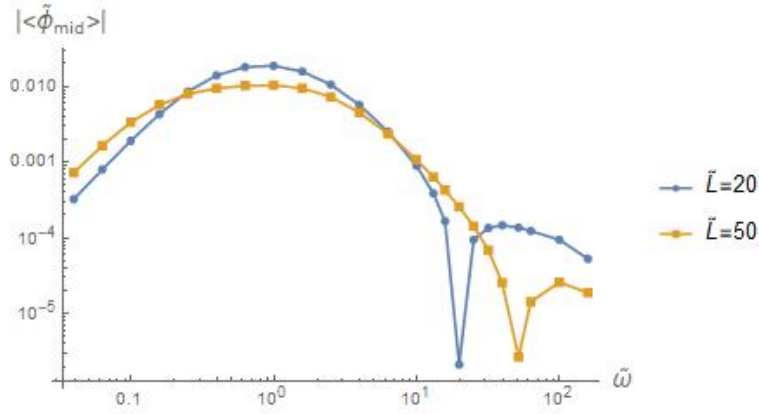
Figure 20: The absolute value of late-time period-average $|\langle \tilde{\phi}_{mid} \rangle|$ as a function of the driving frequency $\tilde{\omega}$ and system size $\tilde{L}$. System parameters: $\phi_0 = 1$, $\frac{D_+}{D_-} = 3$, $\frac{z_+}{z_-} = 1$

We will also run our program with $\frac{D_+}{D_-} = 1$ ($\beta = 0$) and $\frac{z_+}{z_-} = 3$ ($\gamma = \frac{1}{2}$). Ions used in experiments tend not to have valencies higher than 3, so it is unnecessary to model these.
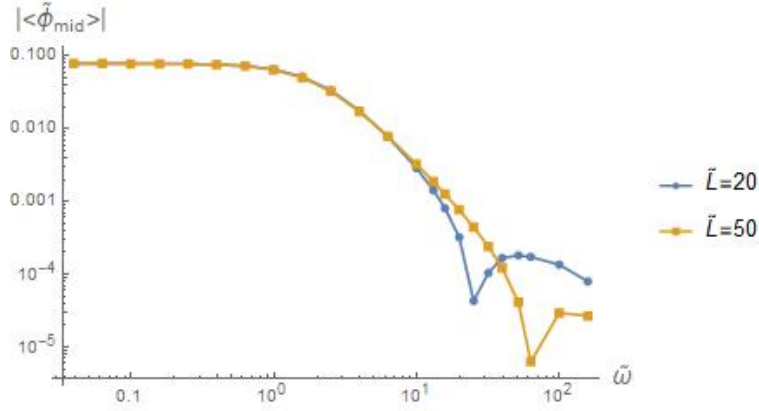
Figure 21: The absolute value of late-time period-average $|\langle \tilde{\phi}_{mid} \rangle|$ as a function of the driving frequency $\tilde{\omega}$ and system size $\tilde{L}$. System parameters: $\phi_0 = 1$, $\frac{D_+}{D_-} = 1$, $\frac{z_+}{z_-} = 3$

At first glance figure 21 may look similar to figure 17, except that on closer inspection we find that the value of the potential at low frequencies is quite a bit higher in figure 21.

To answer our second question, we need to see what happens when we have different diffusion constants and different valencies at the same time. To that end, the next thing we do is set both $\frac{D_+}{D_-}$ and $\frac{z_+}{z_-}$ to 2 (β and γ to $\frac{1}{3}$). The result is shown in figure 22.
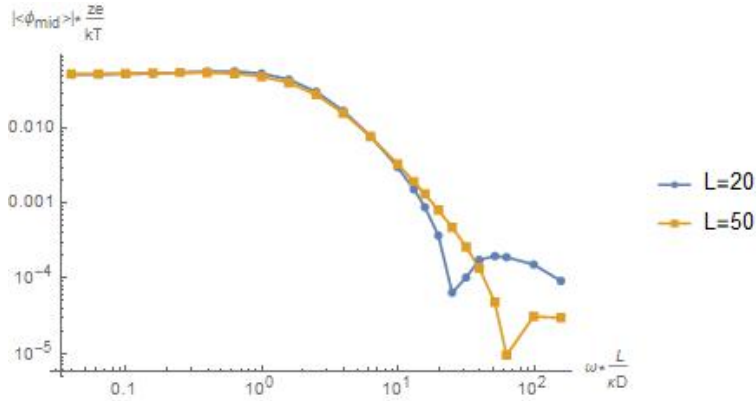
Figure 22: The absolute value of late-time period-average $|\langle \tilde{\phi}_{mid} \rangle|$ as a function of the driving frequency $\tilde{\omega}$ and system size $\tilde{L}$. $\phi_0 = 1$, $\frac{D_+}{D_-} = 2$, $\frac{z_+}{z_-} = 2$

The most notable feature of figure 22 is that it also shows a plateau value of the potential in the low frequency range, rather than decaying to zero. This suggests that the system will always take that value if the valencies are different regardless of whether the diffusion constants are different or not. The average potential only starts to decay once the frequency of the oscillation is sufficiently high that the shape of the double layers shown in figure 18 can no longer fully form. To test this we make some snapshots like those in figure 18 for different frequencies in the $\frac{z_+}{z_-} = \frac{D_+}{D_-} = 2$ case.

(a)   (b)

(c)
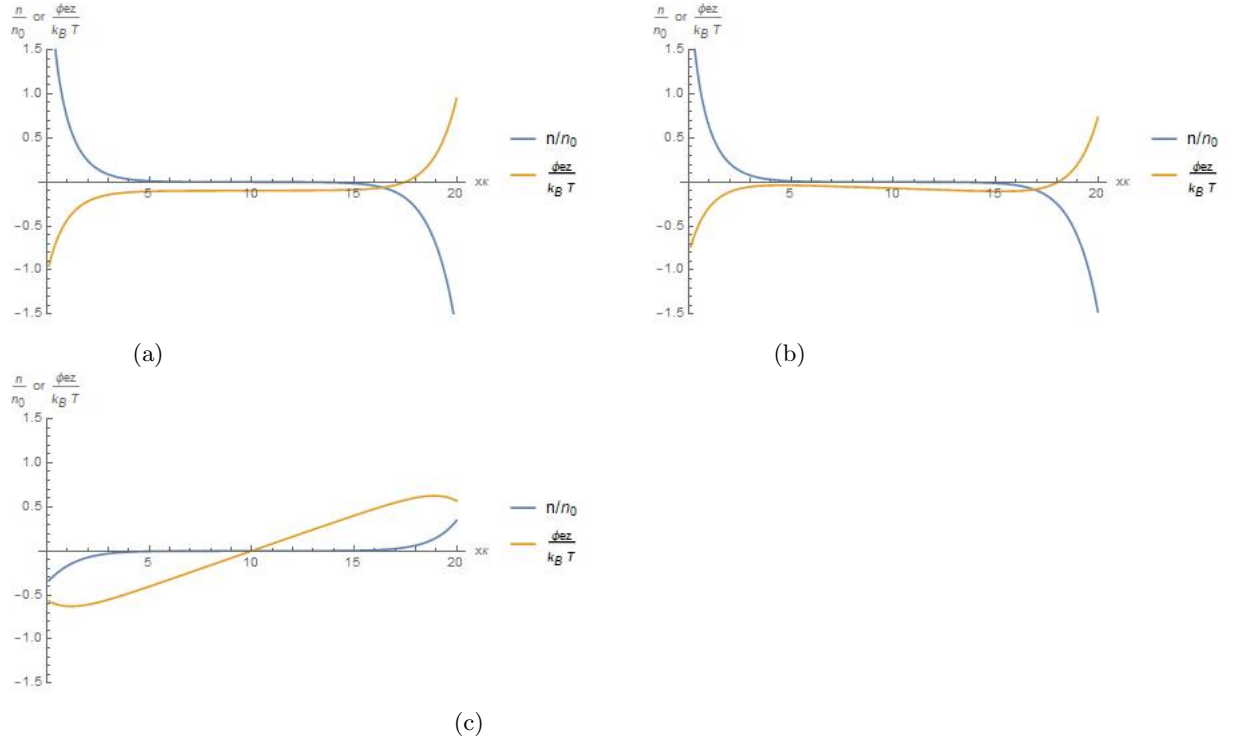
Figure 23: The electric potential ϕ and charge density n as a function of space at one peak of the oscillation for three different frequencies: (a) $\tilde{\omega} = 0.0626131$. (b) $\tilde{\omega} = 0.395062$. (c) $\tilde{\omega} = 2.49267$. For all three: $\frac{z_+}{z_-} = \frac{D_+}{D_-} = 2$, $\tilde{\phi}_0 = 1$, $\tilde{L} = 20$

Figure 23 shows the potential and charge density throughout the system at three different frequencies for $\frac{z_+}{z_-} = \frac{D_+}{D_-} = 2$. It shows how the flat part around the center slowly changes and eventually disappears.

We finish our investigation into different combinations of $\frac{D_+}{D_-}$ and $\frac{z_+}{z_-}$ by combining figures 13, 17, 20, 21, and 22 then adding a few more.
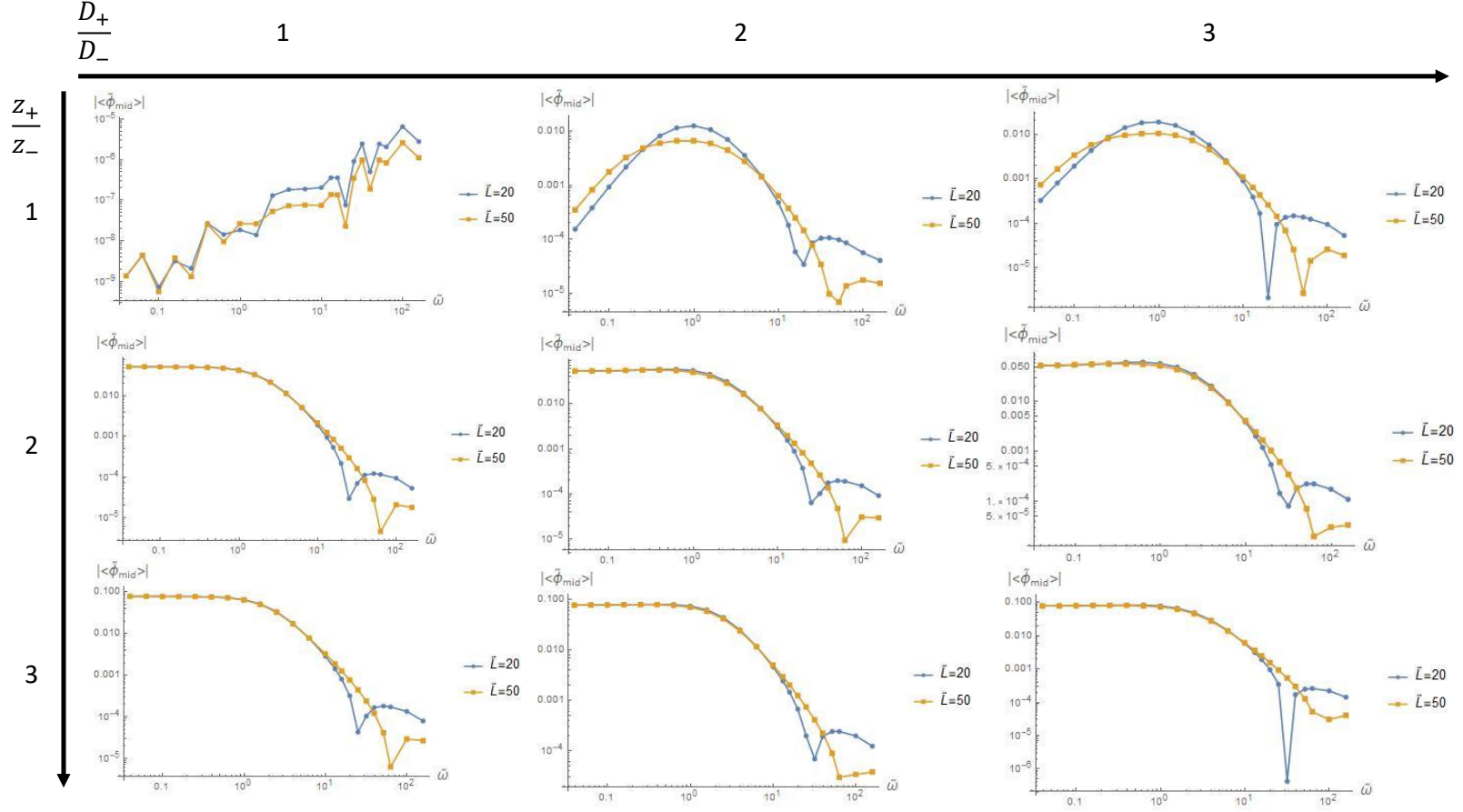
Figure 24: Plots The absolute value of late-time period-average $|\langle \tilde{\phi}_{mid} \rangle|$ as a function of the driving frequency $\tilde{\omega}$ and system size $\tilde{L}$ for several combinations of $\frac{D_+}{D_-}$ and $\frac{z_+}{z_-}$. $\frac{D_+}{D_-}$ increases from left to right. $\frac{z_+}{z_-}$ increases from top to bottom. For all of these: $\tilde{\phi}_0 = 1$

In the following we will refer to the different plots in figure 24 as $(\frac{D_+}{D_-})$ - $(\frac{z_+}{z_-})$. So the top right plot would be 3-1. It may seem pointless to include the 1-1 plot, as in this case the system should be perfectly symmetric and $\langle \phi \rangle = 0$ by symmetry. Specifically because we should not see a finite average potential this plot serves as a measure of the numerical error in our model. We can expect errors of at least the order of magnitude of the value found in the 1-1 plot. The value of the error found at the frequencies where the minimum occurs and above is on the order of the value of the potential found at these high frequencies in the other plots. We have also been unable to find any other research that finds similar high-frequency behaviour. These two factors cast

doubt on the computational accuracy of our program at high frequencies. On the other hand, the consistency with which the minimum appears at $\tilde{\omega} = \tilde{L}$ leads us to believe that this is not simply an error. The 2-1, 2-2. and 2-3 plots show that the plateau value is independent of the diffusion constant. Comparing these three to the 3-1, 3-2, and 3-3 plots we can see that the plateau value does increase with $\frac{z_+}{z_-}$. To see how the plateau value scales with ϕ_0, we plot the 1-2 plot again for $\phi_0 = 0.1$ and $\phi_0 = 10$ in figures 25 and 26 respectively.
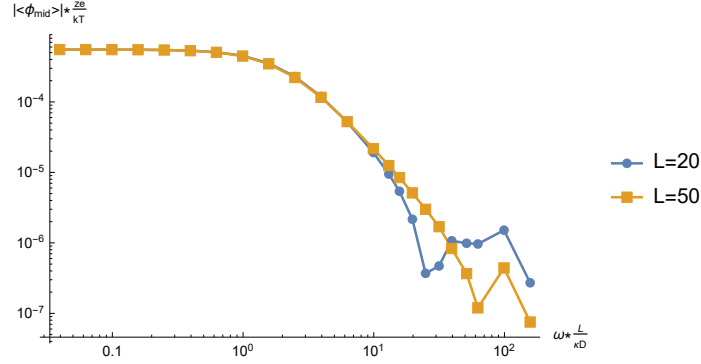
Figure 25: The absolute value of late-time period-average $|\langle \tilde{\phi}_{mid} \rangle|$ as a function of the driving frequency $\tilde{\omega}$ and system size $\tilde{L}$. System parameters: $\phi_0 = 0.1$, $\frac{D_+}{D_-} = 1$, $\frac{z_+}{z_-} = 2$.
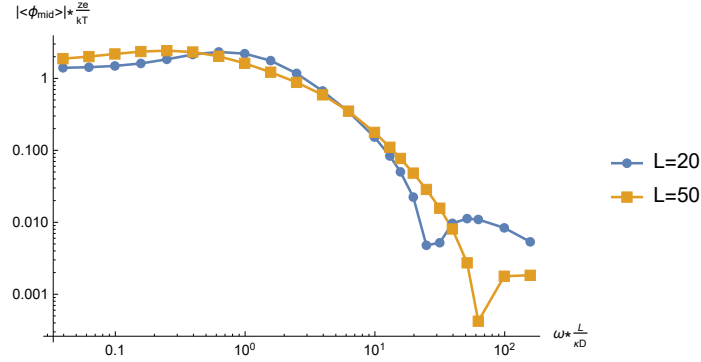
Figure 26: The absolute value of late-time period-average $|\langle \tilde{\phi}_{mid} \rangle|$ as a function of the driving frequency $\tilde{\omega}$ and system size $\tilde{L}$. System parameters: $\phi_0 = 10$, $\frac{D_+}{D_-} = 1$, $\frac{z_+}{z_-} = 2$.

As ϕ_0 goes from 0.1 to 1 and to 10, the plateau value goes from $5 * 10^{-4}$ to $5 * 10^{-2}$ and to $1.5 * 10^0$. The plateau value seems to scale approximately with the square of ϕ_0

5 Conclusion and Discussion

In this thesis, we described a model for solving the Poisson-Nernst-Planck equations. We used this model to study the properties of Asymmetric Rectified Electric Fields in an electrolyte between two planar electrodes with an oscillating potential. Specifically, we studied the value of the electric potential at the center of the system when the cations and anions have different diffusion constants and/or valencies. We averaged this potential over one period of the oscillation after allowing for enough time for transients to disappear. In the low-frequency regime, we found that the average central potential scales with the square of the applied frequency. We also found that it scales with the square of the applied potential, confirming the results by Amrei et al. [6]. The potential is at its highest when the applied frequency is approximately one in units of the RC-frequency. We also found that the potential goes to zero and changes sign when the applied frequency is approximately equal to the length of the system in units of the Debye length. Later tests showed that the numerical accuracy in our model decreases at high frequencies. This could mean that our results for these frequencies are inaccurate, or even wrong. When we used different valencies, we found that the potential takes a constant value in the low-frequency limit. This value increases with the valency difference.

For any applications of these results we recommend avoiding the high frequency regime until experiments or other models can verify or debunk the existence of the sign change. For applications that require large steady fields, using ions with different valencies at frequencies below the RC-frequency seems like the best way to go. The value of the potential has very little frequency dependence and should be easily reproducible over multiple experiments.

6 Appendices

6.1 Debye length

In this section, we will show that our definition of the Debye length (κ^{-1}) is in agreement with the normal definition. In section 3 we defined the Debye length as:

$$\kappa^{-1} = \sqrt{\frac{\epsilon k_B T}{2e^2 z^2 n_0}} \tag{40}$$

where $z = \frac{1}{2}(z_+ - z_-)$ is the valence magnitude defined in section 3 and n_0 is the number density scale defined in eq.(23). Normally, the Debye length is defined as[17]:

$$\kappa^{-1} = \sqrt{\frac{\epsilon k_B T}{e^2(n_{+,0}z_+^2 + n_{-,0}z_-^2)}}. \tag{41}$$

It is easy to see that eqs. (40) and (41) are identical if $z_+ = -z_-$, as the requirement that the system is charge neutral then also requires that $n_{+,0} = n_{-,0}$. However, if the charges are different the equations only match if

$$2z^2 n_0 = n_{+,0}z_+^2 + n_{-,0}z_-^2. \tag{42}$$

In the following, we will show that this is the case.
We start by rewriting the right half of eq.(42) using eq.(23):

$$n_{+,0}z_+^2 + n_{-,0}z_-^2 = \frac{n_0}{1+\gamma}z_+^2 + \frac{n_0}{1-\gamma}z_-^2 = n_0 z_+ \frac{z_+}{1+\gamma} + n_0 z_- \frac{z_-}{1-\gamma}. \tag{43}$$

In the second step, we rearranged some terms to make the next steps more obvious. Now we can use eq.(27) to write:

$$n_0 z_+ \frac{z_+}{1+\gamma} + n_0 z_- \frac{z_-}{1-\gamma} = n_0(z_+ z + z_-(-z)). \tag{44}$$

Finally, we can use the definition of z given above to write:

$$n_0(z_+ z + z_-(-z)) = n_0 z(z_+ - z_-) = n_0 z * (2z) = 2z^2 n_0. \tag{45}$$

This shows that eq.(42) holds, and thus that eq.(40) and eq.(41) are equivalent definitions.

6.2 RC time

We will use this section to derive the expression for the RC time we used in section 3. First, the term RC time refers to the time it takes for a capacitor to charge to $1 - \exp^{-1}$ of its full capacity in a circuit consisting of a resistor(R) and a capacitor(C) in series. The RC time is given by[18]:

$$\tau_{RC} = RC \tag{46}$$

where R is the resistance of the resistor and C is the capacitance of the capacitor. To apply this to our system, we need the resistance and capacitance of the electric double layer:

$$C = \frac{\epsilon\epsilon_0 A}{\kappa^{-1}} \tag{47}$$

$$R = \frac{L}{\sigma A}. \tag{48}$$

$$\tau_{RC} = \frac{\epsilon\epsilon_0 L}{\sigma \kappa^{-1}} \tag{49}$$

Here, ϵ is the relative permittivity of the medium, ϵ_0 is the permittivity of the vacuum, A is the surface area of the electrode, κ^{-1} is the Debye length, L is the distance between the electrodes, and σ is the conductivity of the medium. We have an expression for κ^{-1}, but we still need one for σ. This expression comes in the form of Ohm's law:

$$j = z_+ j_+ + z_- j_- = -\frac{\sigma \nabla \phi}{e}. \tag{50}$$

Here, j is the total electrical current, $\nabla\phi = \frac{\partial \phi}{\partial x}$ is the gradient of the electric potential, and e is the electron charge. This accounts for electrical transport, so we can use the second term on the right-hand side of eq.(21) to write:

$$\sigma = \frac{e^2}{k_B T} \left(D_+ z_+^2 n_+(t,x) + D_- z_-^2 n_-(t,x) \right) \tag{51}$$

Since this must hold for any x and t, we can set $t = 0$ such that eq.(23) applies. Using eq.(23) along with the definition that $z_\pm = z(\gamma \pm 1)$ we can write:

$$\sigma = \frac{e^2 z n_0}{k_B T} \left(D_+ z_+ - D_- z_- \right) \tag{52}$$

We can now use eq.(26), the fact that $\kappa^{-2} = \frac{\epsilon\epsilon_0 k_B T}{2e^2 z^2 n_0}$, and the assumption that $z_+ = -z_- = z$ to get:

$$\sigma = \frac{\epsilon\epsilon_0 D}{2\kappa^{-2}} \left(\frac{1}{1-\beta} - \frac{1}{1+\beta} \right) = \frac{\epsilon\epsilon_0 D}{\kappa^{-2}(1-\beta^2)}. \tag{53}$$

Now we can write the RC time as:

$$\tau_{RC} = \frac{\kappa^{-1} L (1-\beta^2)}{D} = \frac{\kappa^{-1} L}{D_{RC}}, \tag{54}$$

where we defined the effective RC diffusion constant $D_{RC} = \frac{D}{1-\beta^2} = \frac{D_+ + D_-}{2}$

6.3 Matrices B, C, and D

In this section we derive the matrices mentioned in eq.(33). To start, we need to rewrite eq.(29) as a matrix-vector equation:

$$\mathbf{A}\vec{\phi} = \mathbf{B}\vec{q}, \tag{55}$$

where $\vec{\phi}$ is the vector containing the values of ϕ at each grid point, $\vec{q}$ is the vector containing the value of $-\frac{1}{2}((1+\gamma)n_+ - (1-\gamma)n_-)$ at each grid point, and $\mathbf{A}$ and $\mathbf{B}$ are as of yet undetermined matrices. To find these matrices we use the Taylor expansion to rewrite $\phi(x)$:

$$\phi_{k+1} = \phi(x_k+\Delta x) = \phi_k + \frac{d\phi_k}{dx}*\Delta x + \frac{1}{2}\frac{d^2\phi_k}{dx^2}*\Delta x^2 + \frac{1}{6}\frac{d^3\phi_k}{dx^3}*\Delta x^3 + \frac{1}{4!}\frac{d^4\phi_k}{dx^4}*\Delta x^4 + ... \tag{56}$$

$$\phi_{k-1} = \phi_k - \frac{d\phi_k}{dx}*\Delta x + \frac{1}{2}\frac{d^2\phi_k}{dx^2}*\Delta x^2 - \frac{1}{6}\frac{d^3\phi_k}{dx^3}*\Delta x^3 + \frac{1}{4!}\frac{d^4\phi_k}{dx^4}*\Delta x^4 + ... \tag{57}$$

Adding these two equations together and using eq.(29) to write $\frac{d^2\phi_k}{dx^2} = q_k$ we can find:

$$\frac{\phi_{k-1} - 2\phi_k + \phi_{k+1}}{\Delta x^2} = q_k + \frac{1}{12}\frac{d^2 q_k}{dx^2}*\Delta x^2. \tag{58}$$

If we now use a Taylor expansion up to second order for q_k, we find:

$$\frac{d^2 q_k}{dx^2} = \frac{q_{k-1} - 2q_k + q_{k+1}}{\Delta x^2}. \tag{59}$$

We can now define a matrix $D_{i,k} = \frac{\delta_{i,k-1} - 2\delta_{i,k} + \delta_{i,k+1}}{\Delta x^2}$ and write:

$$\mathbf{D}\vec{\phi} = (\mathbb{1} + \frac{\Delta x^2}{12}\mathbf{D})\vec{q}, \tag{60}$$

where $\mathbb{1}$ is the unit matrix.

This is not quite the end, we didn't take the boundary conditions into account. We will assume a set of generic boundary conditions:

$$\phi(z=0) = \Phi_0, \qquad\qquad \phi(z=L) = \Phi_L. \tag{61}$$

Once again we use a Taylor expansion of ϕ to second order

$$\phi_1 = \phi_0 + \frac{d\phi_0}{dx}*\frac{\Delta x}{2} + \frac{1}{2}\frac{d^2\phi_0}{dx^2}*\frac{\Delta x^2}{4} \tag{62}$$

$$\phi_1 = \phi_2 - \frac{d\phi_2}{dx}*\Delta x + \frac{1}{2}\frac{d^2\phi_2}{dx^2}*\Delta x^2. \tag{63}$$

Now we assume that the particles' size means they can't quite reach the boundary. This means $q = 0$ for points close to it. As a consequence: $\frac{d^2\phi_0}{dx^2} = \frac{d^2\phi_2}{dx^2} = 0$, and therefore $\frac{d\phi_0}{dx} = \frac{d\phi_2}{dx}$. Using these assumptions we can combine equations (62) and (63):

$$\frac{\phi_2 - \phi_0}{3\Delta x/2} = \frac{\phi_1 - \phi_0}{\Delta x/2}. \tag{64}$$

We can rewrite this using the boundary condition to get:

$$\phi_2 - 3\phi_1 = -2\Phi_0. \tag{65}$$

We can do the same for the other side of the system:

$$\phi_N = \phi_{N+1} - \frac{d\phi_{N+1}}{dx} * \frac{\Delta x}{2} + \frac{1}{2}\frac{d^2\phi_{N+1}}{dx^2} * \frac{\Delta x^2}{4} \tag{66}$$

$$\phi_N = \phi_{N-1} + \frac{d\phi_{N-1}}{dx} * \Delta x + \frac{1}{2}\frac{d^2\phi_{N-1}}{dx^2} * \Delta x^2 \tag{67}$$

$$\frac{\phi_{N-1} - \phi_{N+1}}{3\Delta x/2} = \frac{\phi_N - \phi_{N+1}}{\Delta x/2} \tag{68}$$

$$\phi_{N-1} - 3\phi_N = -2\Phi_L. \tag{69}$$

With this, we can adapt eq.(60), giving us:

$$\mathbf{D}\vec{\phi} = \mathbf{B}\vec{q} + \vec{C}, \tag{70}$$

where:

$$D_{i,k} = \begin{cases} -\frac{3}{\Delta x^2} & \text{if } i = k = 1 \text{ or } i = k = N \\ \frac{\delta_{i,k-1} - 2\delta_{i,k} + \delta_{i,k+1}}{\Delta x^2} & \text{otherwise} \end{cases} \tag{71}$$

$$\mathbf{B} = \mathbb{1} + \frac{\Delta x^2}{12}\mathbf{D} \tag{72}$$

$$C_i = \begin{cases} \frac{-2\Phi_0}{\Delta x^2} & \text{if } i = 1 \\ \frac{-2\Phi_L}{\Delta x^2} & \text{if } i = N \\ 0 & \text{otherwise.} \end{cases} \tag{73}$$

References

[1] M. Z. Bazant and T. M. Squires, "Induced-charge electrokinetic phenomena: Theory and microfluidic applications," *Phys. Rev. Lett.*, vol. 92, p. 066101, 2004.

[2] V. Studer, A. Pépin, Y. Chen, and A. Ajdari, "An integrated ac electrokinetic pump in a microfluidic loop for fast and tunable flow control," *the Analyst*, vol. 129, pp. 944–949, 2004.

[3] S. Gupta, K. Ramesh, S. Ahmed, and V. Kakkar, "Lab-on-chip technology: A review on design trends and future scope in biomedical applications," *International Journal of Bio-Science and Bio-Technology*, vol. 8, pp. 311–322, 2016.

[4] A. Ajdari, "Pumping liquids using asymmetric electrode arrays," *Physical Review E*, vol. 61, pp. 45–48, 2000.

[5] S. Debesset, C. J. Hayden, C. Dalton, J. C. T. Eijkel, and A. Manz, "An ac electroosmotic micropump for circular chromatographic applications," *Lab on a chip*, vol. 4, pp. 396—-400, 2004.

[6] S. M. H. Hashemi Amrei, S. C. Bukosky, S. P. Rader, W. D. Ristenpart, and G. H. Miller, "Oscillating electric fields in liquids create a long-range steady field," *Phys. Rev. Lett.*, vol. 121, p. 185504, 2018.

[7] S. M. H. H. Amrei, G. H. Miller, and W. D. Ristenpart, "Asymmetric rectified electric fields generate flows that can dominate induced-charge electrokinetics," *Physical Review Fluids*, vol. 5, p. 013702, 2020.

[8] S. M. H. H. A. et al., "*A perturbation solution to the full Poisson–Nernst–Planck equations yields an asymmetric rectified electric field*," *Soft matter*, vol. **16**, pp. 7052–7062, 2020.

[9] S. M. H. H. Amrei, G. H. Miller, and W. D. Ristenpart, "Asymmetric rectified electric fields between parallel electrodes: Numerical and scaling analyses," *PHYSICAL REVIEW E*, vol. 99, pp. 062603–1 – 062603–13, 2019.

[10] R. van Roij, *Lecture notes Soft condensed matter theory*. 2020.

[11] Z. Schuss, B. Nadler, and R. S. Eisenberg, "Derivation of poisson and nernst-planck equations in a bath and channel from a molecular model," *PHYSICAL REVIEW E*, vol. 64, p. 036116, 2001.

[12] S. D. Poisson, "Mémoire sur la théorie du magnétisme en mouvement," *Mémoires de l'Académie Royale des Sciences de l'Institut de France*, vol. 6, p. 441–570, 1823.

[13] W. Nernst, "Zur kinetik der in lösung befindlichen körper," *Zeitschrift Phys Chem*, vol. 2, p. 613–637, 1888.

[14] J. Pedolsky, *Geophysical fluid dynamics*. New York: New York : Springer-Verlag, 1987. 2nd Edition, p. 10.

[15] "Matlab operators and special characters." https://nl.mathworks.com/help/matlab/matlab_prog/matlab-operators-and-special-characters.html, 2021.

[16] J. Crank, *The mathematics of diffusion*. Oxford: Clarendon press, 1975. 2nd Edition, p. 143.

[17] P. Debye and E. Hückel, "Zur theorie der elektrolyte. i. gefrierpunktserniedrigung und verwandte erscheinungen," *Physikalische Zeitschrift*, vol. 24, pp. 185—206, 1923.

[18] S. Dunford, "Calculating the time constant of an rc circuit," *Undergraduate Journal of Mathematical Modeling*, vol. 2, 2010. Article 3.